

Mpemba effects in nonequilibrium open quantum systems

Xuanhua Wang^{1,*} and Jin Wang^{2,3,†}

¹*Center for Theoretical Interdisciplinary Sciences, Wenzhou Institute, University of Chinese Academy of Sciences, Wenzhou, Zhejiang 325001, China*

²*Department of Physics and Astronomy, Stony Brook University, Stony Brook, New York 11794, USA*

³*Department of Chemistry, Stony Brook University, Stony Brook, New York 11794, USA*

Originally, the Mpemba effect (MPE) is referred to the faster icing of a higher-temperature system than a system of a lower temperature. This concept was later generalized to anomalous decays of certain system quantities to the equilibrium states. In this study, we investigate the scenario when a system has no such equilibrium state to approach. Instead, the system is put in contact with two different baths, and only a nonequilibrium state exists, sustained by constant energy injection from the surrounding thermal baths. Firstly, we show that the nonequilibrium conditions can dramatically enlarge the parameter regimes where the MPE emerges. Secondly, we demonstrate that the anomalous MPEs and inverse MPEs emerge in the evolution of quantum correlations in the two-site fermionic system and that nonequilibrium conditions can expedite or delay the MPEs. Thirdly, we show that the nonequilibrium-induced quantum coherence can have considerable contributions to the emergence of the MPE which the conventional Lindbladian dynamics fails to capture.

Introduction.—The anomalous cooling process in which hotter liquids freeze faster than colder liquid has been documented long before the inception of the modern science. The first reported experimental study of the phenomenon in classical systems was conducted in 1960s by Mpemba and Osborne [1], and has triggered heated debates [2, 3]. Mpemba effect (MPE) has been observed in multiple substances by now such as water [4], nanotube resonators [5], granular fluids [6, 7], and Langevin systems [8]. Consequently, the concept of MPE has been generalized from its original context to a broader class of anomalous decays such as the exponentially-accelerated relaxations and the anomalous crossings of many system observables [9, 10]. Recently, seminal works on quantum dot model and spin chains have revealed MPEs in the quantum realm [11–15]. In a classical quasi-static cooling process, the trajectories of a hotter and a cooler systems never intercept according to Newton’s heat law; similarly, in a closed quantum system, the distinctions of states are protected by the unitarity and different states do not intercept in the evolution—a principle known as the conservation of information. Due to the violation of the above principles, it is believed that MPE emerges only in open and strongly nonequilibrium systems [9, 11].

Though multiple mechanisms for MPEs have been hypothesized, whether a universal mechanism for MPEs in different systems exists is not completely clear [16–19]. The first widely applicable mechanism in the Markovian environment was proposed by analyzing the Markovian dynamics of a classical three-level system and the Ising model [9]. The evolution of a system in a Markovian process follows the linear equation

$$\frac{d\vec{p}(t)}{dt} = \mathcal{L}_{T_b}\vec{p}(t) \quad (1)$$

where \mathcal{L}_{T_b} is the linear Markovian operator and T_b is the bath temperature. For a N-level classical system, the Markovian operator can be written using the transition rate matrix R_{ij} , i.e., $\frac{dp_i(t)}{dt} = \sum_j R_{ij}p_j(t)$. This linear equation can be formally

solved by

$$\vec{p}(t) = e^{\hat{R}t}\vec{p}(0) = \sum_i e^{\lambda_i t} \alpha_i \vec{v}_i, \quad (2)$$

where \vec{v}_i is the i -th right eigenvector of the transition matrix \hat{R} and α_i is the coefficient of $\vec{p}(0)$ projecting on \vec{v}_i . The core of the argument is that for certain initial states and bath temperatures T_b , the distribution vector $\vec{p}(0)$ has tiny or zero component on the eigenvector of the slowest decaying mode. This will result in the exponentially faster relaxation of the system compared to a randomly-picked state. Notably, this analysis can be easily generalized into the quantum realm by replacing the distribution function with a density matrix.

In this study, we investigate the scenario in which a quantum system has no equilibrium state to approach. Instead of relaxing to an equilibrium state, the system is in contact with two different baths such that it can only relax to a nonequilibrium steady state (NESS), sustained by constant energy injections from the baths. In this case, we show that the parameter window for observing MPEs can be dramatically widened. Furthermore, we study the evolution of quantum correlations characterized by concurrence and quantum mutual information and investigate the role quantum coherence plays in the dynamics. Quantum coherence is frequently disregarded in the wide-band limit and it decouples from the population terms in the conventional Lindbladian dynamics. Such approximations reduce the quantum property of the system and degrade the quantum density matrix to the one indistinguishable from a classical one. We conduct simulations in both ways with and without quantum coherence. By comparing the two results, we find that the quantum coherence supported by nonequilibrium is capable of qualitatively altering the dynamics and triggering the emergence of MPEs.

Nonequilibrium boost to the MPEs in quantum dot system.—In the previously investigated cases of the Mpemba dynamics, the end states that the systems relax to were mostly chosen to be in equilibrium with the surrounding environments. Naively, it seems that the asymptotic final state a sys-

tem approaches does not influence the emergence of the MPE since the Mpemba crossing occurs during the relaxation process before equilibration. This thinking can be simplistic. The final state is determined by the system parameters and the environment. Given that the environment is the driving force of the system dynamics, its condition can dramatically influence the trajectory of the system evolution as well as the emergence of the MPEs.

To demonstrate this, we consider the quantum dot system coupled with two baths described by the total Hamiltonian $\mathcal{H} = \mathcal{H}_S + \mathcal{H}_R + \mathcal{H}_{int}$ given as follows [20]:

$$\begin{aligned}\mathcal{H}_S &= \sum_{\sigma} \epsilon_0 d_{\sigma}^{\dagger} d_{\sigma} + U n_{\uparrow} n_{\downarrow}, \\ \mathcal{H}_R &= \sum_{k,\sigma} \omega_k a_{k\sigma}^{\dagger} a_{k\sigma} + \sum_{q,\sigma} \omega_q b_{q\sigma}^{\dagger} b_{q\sigma}, \\ \mathcal{H}_{int} &= \sum_{k,\sigma} V (d_{\sigma}^{\dagger} a_{k,\sigma} + d_{\sigma}^{\dagger} b_{k,\sigma}) + \text{h.c.},\end{aligned}\quad (3)$$

where \mathcal{H}_S , \mathcal{H}_R , \mathcal{H}_{int} represent the system Hamiltonian, the Hamiltonian for the two reservoirs and the Hamiltonian for the interaction between the system and the baths, respectively. ϵ_0 is the electron energy in the quantum dot, U is the repulsion energy of electrons, $n_{\sigma} = d_{\sigma}^{\dagger} d_{\sigma}$ is the number operator, and V is the reservoir-system coupling. The creation (annihilation) operators d_{σ}^{\dagger} (d_{σ}) and a_{σ}^{\dagger} (a_{σ}) follow the fermionic statistics $\{d_{\alpha}, d_{\beta}^{\dagger}\} = \delta_{\alpha\beta}$. We write the density matrix as a supervector in the Liouville space representation. The equation of motion of the system is approximated by the quantum master equation

$$\frac{d}{dt} \rho_i(t) = \sum_j M_{ij} \rho_j(t), \quad (4)$$

where the elements of the transition matrix M_{ij} are provided in the Supplemental Material.

One indicator for the emergence of the MPE is the crossing of the density matrix elements. For the quantum dot system, when the two initial states of the systems $\rho^I(0)$ and $\rho^{II}(0)$ are prepared as the steady states with initial preparing baths, the criteria for the crossing of the n -th elements of the density matrices was shown to be $-1 < S_n = \frac{R_{n,3} \Delta a_3}{R_{n,4} \Delta a_4} < 0$ [12], where Δa_i is the difference between the transformed density matrix elements of the two initial states defined by $a_n = \sum_m L_{n,m} \Delta \rho_m(0)$, and $R(L)$ is the right (left) eigenmatrix of the transition matrix. One interesting property of the quantum dot model is that the slowest decaying mode vanishes identically for all initial states in equilibrium with the environment. This suggests an exponential speedup in its decay to the equilibrium state compared to most randomly selected initial states. Notably, this speedup not only holds for the initial states in equilibrium with the baths, but also for the nonequilibrium steady state (NESS) sitting between two baths of different temperatures or chemical potentials.

In the Letter, each quantity associated with the initial preparing baths is indicated by a tilde over the variable. For example, $\tilde{\mu}_{1(2)}$ and $\tilde{\mu}_{3(4)}$ represent the chemical potentials of the preparing baths for the state $\rho^I(0)$ and $\rho^{II}(0)$, respectively.

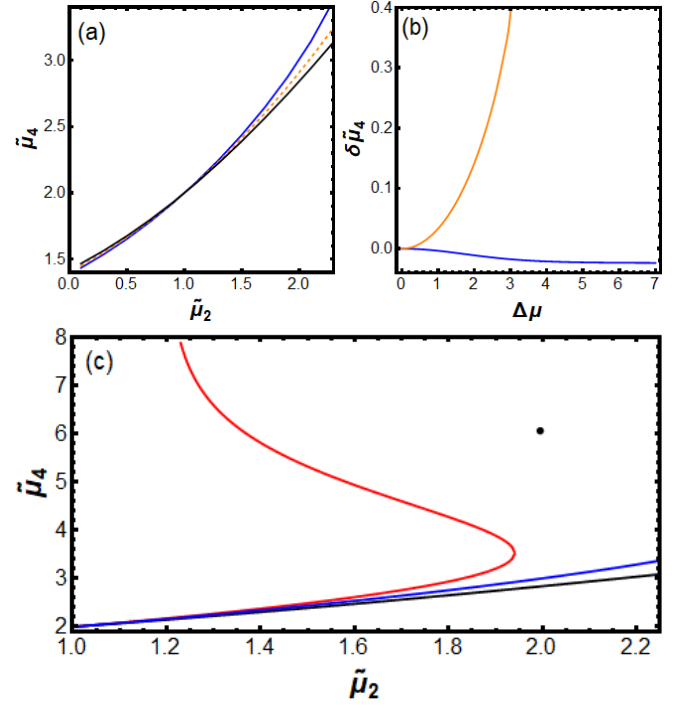


FIG. 1. (a) Boundaries of the preparing chemical potentials that induce QMPE in the equilibrium baths. The parameter regimes in which the QMPE emerges are between the black line ($S_2 = 0$) and the blue line ($S_2 = -1$) intersecting at $(1, 2)$. The dotted orange curve is the solution to $S_2 = -0.2$. The horizontal axis represents the initial preparing chemical potential of one of the baths and the vertical axis represents that of the other bath. Parameters used are $\mu_1 = \mu_2 = 3$. (b) Shifts of the blue boundary ($S_2 = -1$) of (a) due to nonequilibrium baths. The chemical potential of the left preparing bath is fixed at $\tilde{\mu}_2 = 0$ (blue curve) and $\tilde{\mu}_2 = 2$ (orange curve). The two baths that the system is in contact with during relaxation are set to $\mu_1 = 3 - \Delta\mu$, $\mu_2 = 3 + \Delta\mu$. The vertical axis represents the shift of the equilibrium solution represented by the blue curve of Fig. 1 (a) in the nonequilibrium setup. (c) The boundaries of parameter regimes that show QMPE in the nonequilibrium case. In contrast to the narrow range of the Mpemba regime located between the blue and the black curves, the QMPE in nonequilibrium has a much more extended Mpemba regime occupying the entire phase space between the black and the red curves. Parameters used are $\tilde{\mu} = 3$, $\Delta\mu = 4$, $\tilde{\mu}_1 = 2$, $\tilde{\mu}_3 = 1$. For all, $T_1 = T_2 = \tilde{T}_1 = \tilde{T}_2 = \tilde{T}_3 = \tilde{T}_4 = 1$, $\tilde{\mu}_1 = 2$, $\tilde{\mu}_3 = 1$, $\epsilon_0 = 2$, $U = 1.25$.

When the two baths are identical, the parameter regimes where ρ_2 has the Mpemba crossing are shown in Fig. 1 (a). The viable chemical potentials one can use to prepare the initial states that can induce the quantum MPE (QMPE) is within the phase space bounded by the black and the blue curves intersecting at $(\tilde{\mu}_2, \tilde{\mu}_4) = (1, 2)$. This corresponds to the standard QMPE in the relaxation to an equilibrium state. Interestingly, when moved from the equilibrium to the nonequilibrium regimes, one of the boundaries of the Mpemba regimes ($S_2 = 0$) represented by the black curve in Fig. 1 (a) remains unchanged, while the other boundary ($S_2 = -1$) shifts dramatically. The reason is the following. The matrix of the left

eigenvectors L of the transition operator satisfies the condition that

$$L \vec{v} = 0, \quad \text{where} \quad \vec{v} = \{-1, 1, 1, -1\}^T. \quad (5)$$

The equation $S_n = 0$ is satisfied automatically when the vector of initial density matrix elements satisfies the condition $\Delta \vec{\rho}_i \propto \{-1, 1, 1, -1\}^T$. Notably, this condition does not depend on the environmental parameters and is equally applicable to the nonequilibrium case.

To investigate the MPEs in nonequilibrium environments, we vary the chemical potential bias between the two baths [21]. Scanning through $\tilde{\mu}_2$'s, we find that the boundary of the Mpemba regime ($S_2 = -1$) shifts differently before and after the intercepting point $\tilde{\mu}_2 = 1$ as $\Delta\mu$ enlarges – the boundary shifts downwards for $\tilde{\mu}_2 < 1$ and shift upwards for $\tilde{\mu}_2 > 1$ [see Fig. 1 (b)]. This effectively expands the original equilibrium Mpemba regime. An example demonstrating the shifts of the boundary is shown in Fig. 1 (b). Notably, the boundary shift diverges as the chemical potential bias $\Delta\mu$ is enlarged beyond certain threshold. One can numerically determine that the threshold value of the chemical potential bias is $\Delta\mu^* \approx 3.2$. This suggests that when strong nonequilibrium conditions are introduced, i.e., $\Delta\mu > \Delta\mu^*$, an arbitrary large $\tilde{\mu}_4$ will induce the nonequilibrium QMPE. Consequently, the phase space of the Mpemba regime is massively extended. As shown in Fig. 1 (c), the equilibrium QMPE emerges within the regime bounded by the blue and the black curves, and the nonequilibrium condition of the two baths expands the Mpemba regime into one bounded by the red and the black curves. Interestingly, the red curve, which one of the boundaries of the Mpemba regime, ceases to extend beyond a finite $\tilde{\mu}_2$ and leaves the entire regimes on top of the black curve succumbed to the QMPE. This opens up a much broader parameter window for experimental investigations of the QMPE. The evolution of the density matrix elements in the nonequilibrium QMPE regimes exemplified by the black dot in Fig. 1 (c) is demonstrated in the Supplemental Material [22].

Emergence of MPEs in quantum correlations.—Quantum correlations are often viewed as resources for faster quantum processing and play a central role in the quantum thermodynamics and quantum computing [23]. The dynamics of quantum correlations such as the entanglement have been shown to demonstrate peculiar features such as anomalous symmetry restorations and dynamic phase transitions [14, 24–27], and have been one of the focal points of research.

To investigate the dynamics of quantum correlations, we consider a simple bipartite model with two sites. An N -level quantum system truncated to two levels can be easily related to an anti-commuting fermionic system through the Jordan-Wigner transformation [28]. We study the entanglement dynamics of the two-site fermionic system with each site coupled to its own bath. Each site is either occupied by a fermion or vacant and the fermions can tunnel between the two sites. The Hamiltonians of the system \mathcal{H}_S and of the reservoirs \mathcal{H}_R

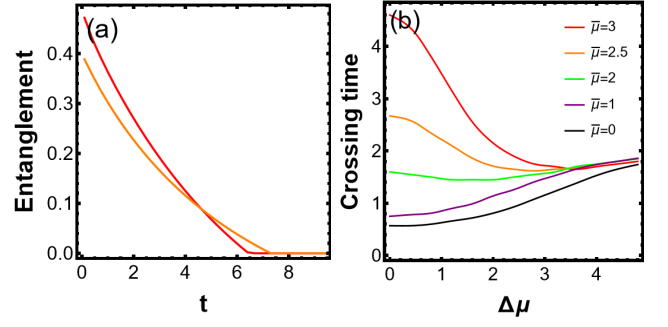


FIG. 2. (a) Evolution of entanglement between the two sites as a function of time. The red curve represents the evolution of the initial state $|\rho^I(0)\rangle = \{0, 0.2, 0.7, 0.1\}$ and the orange curve represents the initial state $|\rho^{II}(0)\rangle = \{0.1, 0.7, 0.1, 0.1\}$. Here, $\mu_1 = \mu_2 = 3$. (b) The time of Mpemba crossing as a function of chemical potential bias $\Delta\mu$. Here, $\mu_1 = \bar{\mu} + \Delta\mu$, $\mu_2 = \bar{\mu} - \Delta\mu$. For both, the parameters used are: $T_1 = T_2 = 1$, $\Gamma = 0.05$, $\omega_1 = \omega_2 = 1$, $\Delta = 0.2$.

are given as follows:

$$\begin{aligned} \mathcal{H}_S &= \sum_{i=1}^2 \omega_i \eta_i^\dagger \eta_i + \Delta (\eta_1^\dagger \eta_2 + \eta_2^\dagger \eta_1), \\ \mathcal{H}_R &= \sum_{k,p} \omega_k (a_{kp}^\dagger a_{kp}) + \sum_{q,s} \omega_q (b_{qs}^\dagger b_{qs}), \end{aligned} \quad (6)$$

where Δ is the hopping rate between the two sites, η_i^\dagger (η_i) is the creation (annihilation) operator on the i -th site which follows the standard fermionic statistics. The interaction Hamiltonian between the system and the two reservoirs is given by

$$\mathcal{H}_{int} = \sum_{k,p} \lambda_k (\eta_1^\dagger a_{kp} + \eta_1 a_{kp}^\dagger) + \sum_{q,s} \lambda_q (\eta_2^\dagger b_{qs} + \eta_2 b_{qs}^\dagger), \quad (7)$$

where λ is the interaction strength between the system and the reservoir and a_{kp}^\dagger (b_{qs}^\dagger) is the creation operator for a particle of momentum k , polarization p from the reservoir.

For simplicity, we consider the symmetric case $\omega_1 = \omega_2 = 1$. In this case, the eigenvalues of the transition matrix of its Lindblad equation are independent of the tunneling rate and are given by

$$\lambda_1 = -4\Gamma, \quad \lambda_2 = \lambda_3 = -2\Gamma, \quad \lambda_4 = 0. \quad (8)$$

The transition matrix M is diagonalizable and the vectorized density operator can be expressed as

$$\vec{\rho}(t) = \sum_i e^{\lambda_i t} \alpha_i(0) \vec{v}_i, \quad (9)$$

where \vec{v}_i is the i -th eigenvector of the transition matrix and $\alpha_i(0)$ is the coefficient of the i -th eigenvector defined by $\alpha_i(0) = \langle \vec{\delta}_i, \vec{\rho}(0) \rangle$. The matrix of vectors $\{\vec{\delta}_i\}$ is the inverse of the matrix of eigenvectors $\{\vec{v}_i\}$.

Usually, to have the “strong Mpemba effect”, the coefficient of the slowest decaying mode is required to vanish for the particularly chosen initial conditions. In this model, both $\alpha_2(0)$

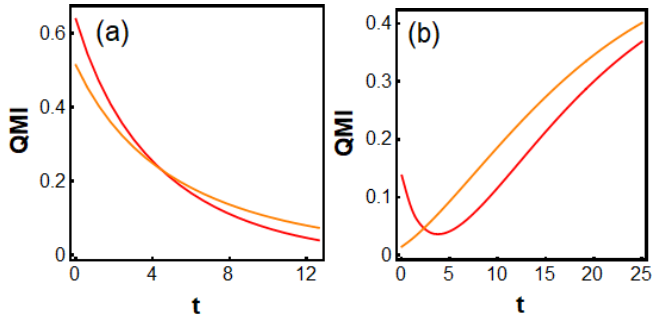


FIG. 3. MPE and inverse MPE in the evolutions of the QMI between the two sites. (a) The red curve represents the evolution of the initial state $|\rho^I(0)\rangle = \{0.1, 0.1, 0.7, 0.1\}$ and the orange curve is for the initial state $|\rho^H(0)\rangle = \{0.1, 0.65, 0.1, 0.15\}$. Parameters used are: $T_1 = T_2 = 1$, $\mu_1 = \mu_2 = 3$. (b) The red curve represents the evolution of the initial state $|\rho(0)\rangle = \{0.4, 0.1, 0.2, 0.3\}$ and the orange curve is for the initial state $|\rho(0)\rangle = \{0.3, 0.3, 0.2, 0.2\}$. Parameters used are: $T_1 = T_2 = 0.1$, $\mu_1 = \mu_2 = 1.2$. For both, $\Gamma = 0.05$, $\omega_1 = \omega_2 = 1$, $\Delta = 0.2$.

and $\alpha_3(0)$ need to vanish due to the degeneracy of the eigenvalue. This gives the condition $\langle \delta_2, \vec{\rho}(0) \rangle = \langle \delta_3, \vec{\rho}(0) \rangle = 0$ where the vector δ_2 and δ_3 are given in the Supplemental Material. Notably, the strong MPE refers the exponentially faster equilibration towards the equilibrium state, but does not guarantee the emergence of the anomalous crossing. For the nonequilibrium systems with multiple baths, a similar “strong Mpemba effect” can be defined for systems that show exponentially faster decay to the NESS with vanishing coefficients for the slowest decaying mode. This coefficient now depends on the parameters of both of the two baths. Generally, it is not necessary for a system to satisfy the strong Mpemba condition to manifest crossings of interested physical quantities during the relaxation.

To demonstrate the dynamical behaviors of quantum correlations in the system, we introduce the concurrence and the quantum mutual information (QMI) between the two subsystems. The concurrence is an entanglement monotone derived from the entanglement formation [29, 30]. For the system we consider, the concurrence can be simplified to

$$\mathcal{E}(\rho) = 2 \max(0, |\rho'_{22}| - \sqrt{\rho'_{11}\rho'_{44}}), \quad (10)$$

where ρ'_{ij} are the entries of the density matrix in local basis. Another widely-used measure of correlations is the QMI, which is a direct generalization of classical mutual information and quantifies the maximum amount of information that can be securely transferred between two parties [31, 32]. For a bipartite system AB with the density operator ρ^{AB} and the subsystem $A(B)$ with the reduced density operator $\rho^{A(B)} = \text{Tr}_{B(A)}(\rho^{AB})$, the QMI is defined as

$$\mathcal{I}(\rho^{AB}) = S(\rho^A) + S(\rho^B) - S(\rho^{AB}), \quad (11)$$

where $S(\rho) = -\text{tr}(\rho \log_2 \rho)$ is the von Neumann entropy.

The dynamics of the entanglement and the QMI for our system are shown in Fig. 2 and 3. In Fig. 2, we demonstrate the

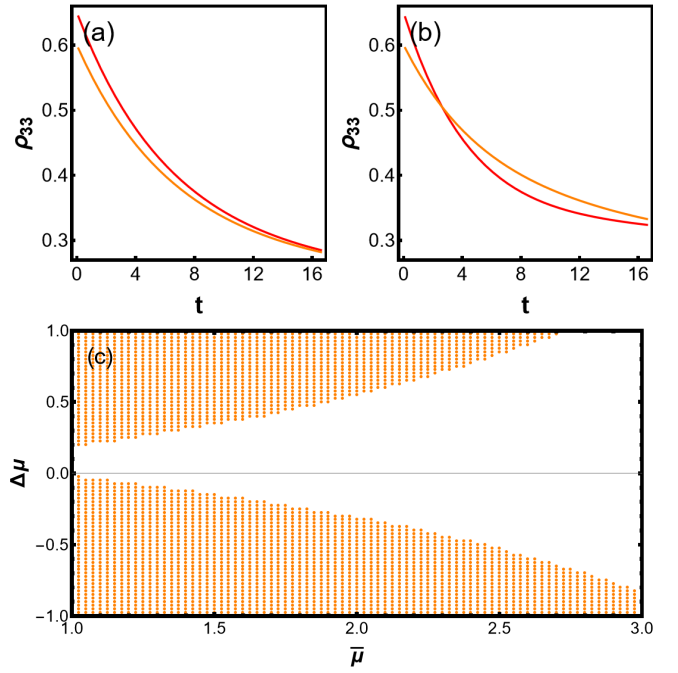


FIG. 4. Evolution of the density matrix element ρ_{33} as a function of time with and without coherence terms. (a) The population dynamics without the coherence terms. (b) The population dynamics with the coherence terms. The off-diagonal terms in the initial condition are chosen at $\rho_{23} = \rho_{32} = 0.2$ for the red curve and $\rho_{23} = \rho_{32} = -0.1$ for the orange curve. For both (a) and (b), the population terms are identical. The red curve represents the evolution of the initial state with the population terms $|\rho^I(0)\rangle = \{0.1, 0.25, 0.65, 0\}$ and the orange curve is for the initial state with the population terms $|\rho^H(0)\rangle = \{0.1, 0.2, 0.6, 0.1\}$. (c) The shaded region in orange represents the MPE regime of (b) with $\mu_{1,2} = \bar{\mu} \pm \Delta\mu$. Parameters used are: $T_1 = T_2 = 1$, $\mu_1 = 0.1$, $\mu_2 = 3$, $\Gamma = 0.05$, $\omega_1 = \omega_2 = 1$, $\Delta = 0.05$.

emergence of the MPE in the entanglement evolution from two different initial states. The initially more entangled state, represented by the red curve in Fig. 2 (a), has a faster rate of disentanglement and disentangles earlier than the state that is initially less entangled. This represents possible tradeoffs between the entangling time and the entangling strength for quantum states. In addition, the vanishing of entanglement within a finite time has been observed in various systems and is termed the “sudden death” in contrast to the smooth asymptotic decay observed in the dynamics of QMI [33]. As shown in Fig. 2 (b), the nonequilibrium condition can significantly influence the crossing time of the entanglements and advance it when the average chemical potential of the baths is large. This effect can be intuitively understood as follows. When the baths are set at large μ 's, the quantum states are approximately fully occupied. Increasing the bias in this case means lowering the occupation of one of the bath while keeping the occupation of the other bath roughly unchanged. In this case, the state $\rho^I(0)$ which has a higher excitation energy obtains a higher rate of decay, resulting in an earlier crossing time. On the other hand, for very low chemical potentials the fermion states are approximately vacant. Enlarging $\Delta\mu$

effectively raises the occupation number of one of the baths while leaves the other bath unchanged. This increase of the chemical potential causes a slower decay and a delayed crossing time. The same argument explains why the crossing time approaches a constant for extremely large chemical potential biases regardless of the average potentials. In Fig. 3, we show the MPE and the inverse MPE in the evolution of the QMI. These two figures jointly demonstrate the ubiquity of Mpemba crossings in the evolution of quantum systems.

Influence from the quantum coherence.—One of the essential features of a quantum system is the existence of the off-diagonal coherence terms, which differentiate its density matrix from a classical one [34]. In the conventional Lindbladian treatment, the coherence terms represented by the off-diagonal elements in the density matrix decouple with the population terms in the dynamics. Under the wide-band approximation frequently used in quantum dot systems, the coherence terms are erased completely. For a quantum system out of equilibrium and in contact with multiple baths, these ignored quantum coherence can play a significant role in the system dynamics, especially when the tunneling rate is comparable to the decoherence rate [35–37]. We show that in weak tunneling regimes, the quantum coherence can give rise to the emergence of QMPE while the population dynamics without it predicts the otherwise. This distinctive feature caused by coherence can only take place when strong nonequilibrium conditions are introduced.

In Fig. 4 (a) and (b), we show explicitly that in the regime where no sign of the QMPE is witnessed when the coherence is ignored, the QMPE emerges when coherence is considered. Furthermore, the emergence of QMPE is only possible when an intrinsic nonequilibrium condition is introduced. As shown in Fig. 4 (c), for larger average potentials $\bar{\mu}$'s, larger $\Delta\mu$'s are required for the emergence the QMPE. This is due to the fact that larger biases are necessary to substantially alter the

occupation number of the baths at high chemical potentials. Small biases fail to create enough differences from the equilibrium solutions, consequently, do not generate enough coherence necessary to trigger the QMPE. This is a demonstration that quantum coherence can have qualitative influence on the dynamics of the system. Importantly, the magnitude of the quantum coherence is amplified in the weak tunneling regimes and its asymptotic value is approximately proportional to the bias between the baths occupation numbers [35]. Therefore, this “coherence-induced MPE” is an intrinsic nonequilibrium phenomenon that only emerges when the multiple supporting baths of subsystems are different and it is most conspicuous when the tunneling rate of the fermions is not significantly larger than the decay rate ($\Delta \lesssim 2\Gamma$).

Conclusion.—In this study, we investigated the quantum Mpemba effect in the quantum dot and the two-site fermion systems coupled with two different baths. Firstly, we showed that nonequilibrium conditions can dramatically expand the parameter space where the MPE emerges. This opens up a much wider window both conceptually and also practically for experimental investigations. Secondly, we investigated the dynamics of quantum correlations in the two-fermionic system coupled with two different baths and showed that anomalous decays of MPEs and inverse MPEs emerge in the evolution of the entanglement and the QMI. We demonstrated that nonequilibrium conditions can significantly influence the times of the Mpemba crossings. Thirdly, we studied the possible influence on the dynamics due to the nonequilibrium-induced quantum coherence which is absent in the conventional Lindbladian dynamics. Our results show that in the weak tunneling regimes, the quantum coherence, which is supported by the nonequilibrium conditions of the two baths, has nontrivial influence the population dynamics and can induce the emergence of the QMPE which the population dynamics alone fail to predict.

SUPPLEMENTAL MATERIAL

In the Supplemental Material, we provide certain calculation details of the quantum dot and the two fermion models in the main text as well as extra figures on the MPEs in the quantum dot system.

MPE in the quantum dot model

The Lindblad equation of the quantum dot model has been studied in many previous papers [12, 38, 39]. The results we used in this study are summarized in this section which can be found in Refs. [12, 13, 40]. The four spin configurations – the doubly-occupied state, two singly-occupied states, and empty state – are labeled by $\alpha = 1, 2, 3, 4$, respectively. Under the wide-band approximation, the density matrix ρ reduces to a diagonal form with the four matrix elements whose vectorized form is represented by ρ_α . The quantum Master equation of the vector is given by

$$\frac{d}{dt}\rho_i = \sum_j M_{ij}\rho_j, \quad (12)$$

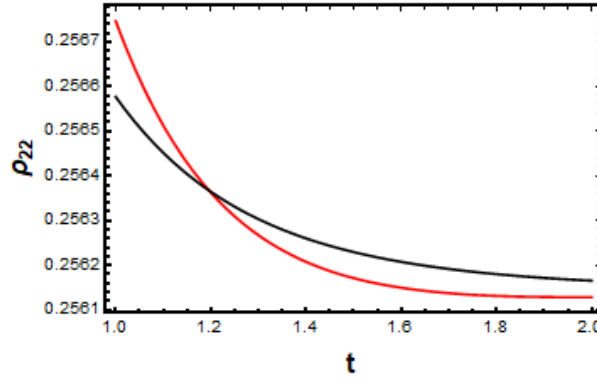


FIG. 5. Example of the evolution of the density matrix element ρ_{22} at the $(\tilde{\mu}_2, \tilde{\mu}_4) = (2, 6)$ indicated by the black dot in Fig. 1 (c). Parameters used are $T_1 = T_2 = \tilde{T}_1 = \tilde{T}_2 = \tilde{T}_3 = \tilde{T}_4 = 1$, $\tilde{\mu} = 3$, $\Delta\mu = 4$, $\tilde{\mu}_1 = 2$, $\tilde{\mu}_3 = 1$.

where the transition matrix is given by [12]

$$M_{ij} = \begin{pmatrix} -2(2 - f^{(1)}) & f^{(1)} & f^{(1)} & 0 \\ (2 - f^{(1)}) & -(2 - f^{(0)}) - f^{(1)} & 0 & f^{(0)} \\ (2 - f^{(1)}) & 0 & -(2 - f^{(0)}) - f^{(1)} & f^{(0)} \\ 0 & (2 - f^{(0)}) & (2 - f^{(0)}) & -2f^{(0)} \end{pmatrix}. \quad (13)$$

Here, we have set the decay rate to $\Gamma = 1$. $f^{(j)}$ with $j = 0, 1$ is defined as the sum of fermionic occupation numbers of the two baths $f^{(j)} = \frac{1}{1 + e^{(\epsilon_0 + jU - \mu_L)/T}} + \frac{1}{1 + e^{(\epsilon_0 + jU - \mu_R)/T}}$, where $\mu_{L(R)}$ represents the chemical potential of the left (right) bath. The time evolution of the density matrix element $\rho_\alpha(t)$ is given by

$$\rho_\alpha(t) = \sum_{n=1}^4 e^{\lambda_n t} R_{\alpha n} a_n, \quad (14)$$

where $a_n = \sum_{m=1}^4 L_{nm} \rho_m(0)$, λ_n represents the eigenvalue of the transition matrix M , and $L_{ij}(R_{ij})$ represents the matrix of left (right) eigenvectors the transition matrix given as follows:

$$R = \begin{pmatrix} \frac{f^{(0)} f^{(1)}}{4+2(f^{(0)}-f^{(1)})} & 0 & \frac{2f^{(0)} f^{(1)}}{-4+(f^{(0)}-f^{(1)})^2} & \frac{f^{(0)} f^{(1)}}{4-2(f^{(0)}-f^{(1)})} \\ \frac{f^{(0)}(2-f^{(1)})}{4+2(f^{(0)}-f^{(1)})} & -\frac{1}{2} & -\frac{f^{(0)}(2-f^{(0)}-f^{(1)})}{-4+(f^{(0)}-f^{(1)})^2} & -\frac{f^{(0)} f^{(1)}}{4-2(f^{(0)}-f^{(1)})} \\ \frac{f^{(0)}(2-f^{(1)})}{4+2(f^{(0)}-f^{(1)})} & \frac{1}{2} & -\frac{f^{(0)}(2-f^{(0)}-f^{(1)})}{-4+(f^{(0)}-f^{(1)})^2} & -\frac{f^{(0)} f^{(1)}}{4-2(f^{(0)}-f^{(1)})} \\ \frac{(2-f^{(0)})(2-f^{(1)})}{4+2(f^{(0)}-f^{(1)})} & 0 & -\frac{2f^{(0)}(2-f^{(0)})}{-4+(f^{(0)}-f^{(1)})^2} & \frac{f^{(0)} f^{(1)}}{4-2(f^{(0)}-f^{(1)})} \end{pmatrix}, \quad (15)$$

and

$$L = \begin{pmatrix} 1 & 1 & 1 & 1 \\ 0 & -1 & 1 & 0 \\ -\frac{2-f^{(1)}}{f^{(0)}} & -\frac{2-f^{(0)}-f^{(1)}}{2f^{(0)}} & -\frac{2-f^{(0)}-f^{(1)}}{2f^{(0)}} & 1 \\ \frac{(2-f^{(0)})(2-f^{(1)})}{f^{(0)} f^{(1)}} & -\frac{2-f^{(0)}}{f^{(0)}} & -\frac{2-f^{(0)}}{f^{(0)}} & 1 \end{pmatrix}. \quad (16)$$

In Fig. 5, we show the example of the QMPE at $(\tilde{\mu}_2, \tilde{\mu}_4) = (2, 6)$ indicated by the black dot in Fig. 1 (c) in the main body. In Fig. 6, we show that the vast extension of parameter space of the Mpemba regime also exists for the other singly-occupied state ρ_3 . For the doubly-occupied and vacant states, the nonequilibrium condition has no influence on the Mpemba regime.

MPE in the two fermion model

In the energy eigenbasis, the master equation for the density matrix is

$$\frac{d}{dt} \rho_{ij} = \sum_{kl} M_{ij}^{kl} \rho_{kl}. \quad (17)$$

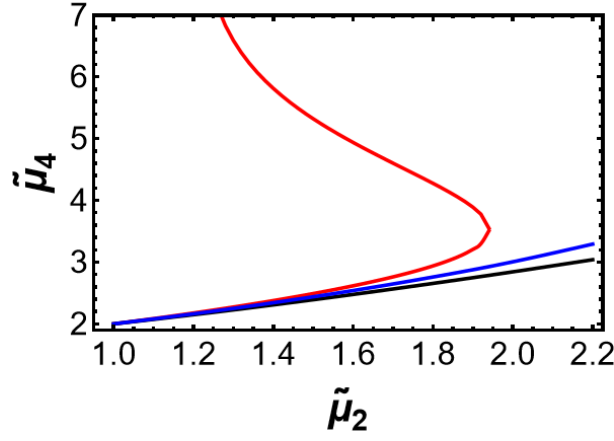


FIG. 6. The boundaries of parameter regime that show QMPE for the third density matrix element ρ_3 ($-1 < S_3 < 0$). The Mpemba regime in the equilibrium environment expands between the blue and the black curves, and the QMPE in nonequilibrium extends to the parameter space between the black and the red curves. Parameters used are $\bar{\mu} = 3$, $\Delta\mu = 4$, $\tilde{\mu}_1 = 2$, $\tilde{\mu}_3 = 1$. For all, $T_1 = T_2 = \tilde{T}_1 = \tilde{T}_2 = \tilde{T}_3 = \tilde{T}_4 = 1$, $\tilde{\mu}_1 = 2$, $\tilde{\mu}_3 = 1$, $\epsilon_0 = 2$, $U = 1.25$.

The nonzero matrix elements M_{ij}^{lk} for fermionic reservoirs without consideration of the quantum coherence terms are given as follows,

$$M_{11}^{11} = -2(\Gamma_1(\sin^2(\theta/2)n_1^{T_1} + \cos^2(\theta/2)n_1^{T_2}) + \Gamma_2(\cos^2(\theta/2)n_2^{T_1} + \sin^2(\theta/2)n_2^{T_2})), \quad (18)$$

$$M_{11}^{22} = -2\Gamma_1(\sin^2(\theta/2)n_1^{T_1} + \cos^2(\theta/2)n_1^{T_2}) + 2\Gamma_1, \quad (19)$$

$$M_{11}^{33} = -2\Gamma_2(\cos^2(\theta/2)n_2^{T_1} + \sin^2(\theta/2)n_2^{T_2}) + 2\Gamma_2, \quad (20)$$

$$M_{22}^{11} = -M_{11}^{22} + 2\Gamma_1, \quad (21)$$

$$M_{22}^{22} = -M_{11}^{22} + M_{11}^{33} - 2\Gamma_2, \quad (22)$$

$$M_{22}^{44} = M_{11}^{33}, \quad (23)$$

$$M_{33}^{11} = 2\Gamma_2(\cos^2(\theta/2)n_2^{T_1} + \sin^2(\theta/2)n_2^{T_2}), \quad (24)$$

$$M_{33}^{33} = M_{11}^{22} - 2\Gamma_1 - M_{11}^{33}, \quad (25)$$

$$M_{33}^{44} = M_{11}^{22}, \quad (26)$$

$$M_{44}^{22} = M_{33}^{11}, \quad (27)$$

$$M_{44}^{33} = M_{22}^{11}, \quad (28)$$

$$M_{44}^{44} = -M_{11}^{22} - M_{11}^{33}, \quad (29)$$

$$\text{where } \cos\theta = \frac{\omega_2 - \omega_1}{\sqrt{(\omega_1 - \omega_2)^2 + 4\Delta^2}}.$$

The time evolution of the vectorized density operator is given by

$$\vec{\rho}(t) = \sum_i e^{\lambda_i t} \alpha_i(0) \vec{v}_i, \quad (30)$$

where \vec{v}_i is the i -th eigenvector of the transition matrix and $\alpha_i(0)$ is the coefficient of the i -th eigenvector defined by $\alpha_i(0) = \langle \vec{\delta}_i, \vec{\rho}(0) \rangle$. The matrix of vectors $\{\vec{\delta}_i\}$ is the inverse of the matrix of eigenvectors $\{\vec{v}_i\}$. The matrix of the row vectors of $\vec{\delta}_i$'s is given by

$$\begin{pmatrix} \frac{1}{4}n_{1p}n_{2p} & \frac{1}{4}(n_{1p}-2)n_{2p} & \frac{1}{4}n_{1p}(n_{2p}-2) & \frac{1}{4}(n_{1p}-2)(n_{2p}-2) \\ -\frac{1}{2}(n_{1p}n_{2p}) & -\frac{1}{2}(n_{1p}-1)n_{2p} & -\frac{1}{2}n_{1p}(n_{2p}-1) & \frac{1}{2}(-n_{2p}n_{1p} + n_{1p} + n_{2p}) \\ \frac{1}{2}(n_{1p}-1)n_{2p} & \frac{1}{2}(n_{1p}-2)n_{2p} & \frac{1}{2}(n_{1p}(n_{2p}-1) - n_{2p} + 2) & \frac{1}{2}(n_{1p}-2)(n_{2p}-1) \\ \frac{1}{4}n_{1p}n_{2p} & \frac{1}{4}n_{1p}n_{2p} & \frac{1}{4}n_{1p}n_{2p} & \frac{1}{4}n_{1p}n_{2p} \end{pmatrix}, \quad (31)$$

where $n_{ip} = n(\omega'_i, T_1) + n(\omega'_i, T_2)$.

When the quantum coherence terms are included, the equations of motion can be computed by the Redfield equation, which is the equation of motion of the density operator with the coherence coupling considered. The matrix elements M_{ij}^{lk} for the population terms are the same as the ones above. The elements involving coherence couplings are given as follows [35]:

$$M_{11}^{23} = M_{11}^{32} = -\sin(\theta/2)\cos(\theta/2)(\Gamma_1(n_1^{T_1} - n_1^{T_2}) + \Gamma_2(n_2^{T_1} - n_2^{T_2})), \quad (32)$$

$$M_{22}^{23} = M_{22}^{32} = M_{33}^{23} = M_{33}^{32} = M_{23}^{11} = M_{23}^{22} = M_{23}^{33} = M_{23}^{44} = -M_{11}^{23}, \quad (33)$$

$$M_{44}^{23} = M_{44}^{32} = M_{11}^{23}, \quad (34)$$

$$M_{23}^{32} = -\Gamma_1 - \Gamma_2 + i(\omega'_2 - \omega'_1). \quad (35)$$

Here, $\omega'_{1,2} = \frac{1}{2}(\omega_1 + \omega_2 \pm \sqrt{(\omega_1 - \omega_2)^2 + 4\Delta^2})$, $M_{32}^{lk} = (M_{23}^{lk})^*$ for all l, k and the rest of the matrix elements are zero.

The eigenvalues of the transition matrix is given by

$$\lambda_1 = -4\Gamma, \lambda_2 = \lambda_3 = -2\Gamma, \lambda_{4,5} = -2\Gamma \pm 2\Delta i, \lambda_6 = 0. \quad (36)$$

Notably, the transition matrix has two additional complex eigenvalues λ_4 and λ_5 in comparison with that in the Lindbladian dynamics. The imaginary parts in the eigenvalues result in more oscillatory behaviors in the dynamics which can postpone or advance the time of the Mpemba crossing. Importantly, under the wide-band approximation in the Lindbladian formalism, the system is characterized by the population terms in the density matrix. This form of density matrix has a classical correspondence of the probability distribution and its dynamics has a classical interpretation. The conventional Lindblad equation uses the secular approximation to decouple the coherence terms from the population terms. However, the quantum coherence terms, which does not have the classical counterpart, can couple directly with the population terms in the Redfield equation and can influence the population dynamics in a nontrivial way.

The basis transformation is explicitly given as follows. For the symmetric site case, i.e. $\omega_1 = \omega_2$, the transformation from the global to the local basis is given by

$$\rho_{\text{local}} = U\rho U^\dagger = \begin{pmatrix} \rho_{11} & 0 & 0 & 0 \\ 0 & \frac{1}{2}(\rho_{22} + \rho_{33}) - \text{Re}(\rho_{23}) & -\frac{1}{2}(\rho_{22} - \rho_{33}) + \text{Im}(\rho_{23}) & 0 \\ 0 & -\frac{1}{2}(\rho_{22} - \rho_{33}) - \text{Im}(\rho_{23}) & \frac{1}{2}(\rho_{22} + \rho_{33}) + \text{Re}(\rho_{23}) & 0 \\ 0 & 0 & 0 & \rho_{44} \end{pmatrix}, \quad (37)$$

where ρ_{ij} in the matrix is evaluated in the energy eigenbasis. The concurrence written in the eigenbasis of the system Hamiltonian \mathcal{H}_S is given by

$$\mathcal{E}(\rho) = 2 \max(0, |\rho_{22} - \rho_{33}| - \sqrt{\rho_{11}\rho_{44}}). \quad (38)$$

* wangxh@ucas.ac.cn

† Corresponding author: jin.wang.1@stonybrook.edu

- [1] E. B. Mpemba and D. G. Osborne, Cool?, *Physics Education* **4**, 172 (1969).
- [2] J. Bechhoefer, A. Kumar, and R. Ch  trite, A fresh understanding of the mpemba effect, *Nature Reviews Physics* **3**, 534 (2021).
- [3] H. C. Burridge and P. F. Linden, Questioning the mpemba effect: Hot water does not cool more quickly than cold, *Scientific Reports* **6**, 1 (2016).
- [4] M. Jeng, The mpemba effect: When can hot water freeze faster than cold?, *American Journal of Physics* **74**, 514 (2006).
- [5] P. A. Greaney, G. Lani, G. Cicero, and J. C. Grossman, Mpemba-like behavior in carbon nanotube resonators, *Metalurgical and Materials Transactions A* **42**, 3907 (2011).
- [6] A. Lasanta, F. V. Reyes, A. Prados, and A. Santos, When the hotter cools more quickly: Mpemba effect in granular fluids, *Physical review letters* **119**, 148001 (2017).
- [7] A. Biswas, V. Prasad, O. Raz, and R. Rajesh, Mpemba effect in driven granular maxwell gases, *Physical Review E* **102**, 012906 (2020).
- [8] A. Biswas, R. Rajesh, and A. Pal, Mpemba effect in a langevin system: Population statistics, metastability, and other exact results, *The Journal of Chemical Physics* **159** (2023).
- [9] Z. Lu and O. Raz, Nonequilibrium thermodynamics of the markovian mpemba effect and its inverse, *Proceedings of the National Academy of Sciences* **114**, 5083 (2017).
- [10] I. Klich, O. Raz, O. Hirschberg, and M. Vucelja, Mpemba index and anomalous relaxation, *Physical Review X* **9**, 021060 (2019).
- [11] F. Carollo, A. Lasanta, and I. Lesanovsky, Exponentially accelerated approach to stationarity in markovian open quantum systems through the mpemba effect, *Physical Review Letters* **127**, 060401 (2021).
- [12] A. K. Chatterjee, S. Takada, and H. Hayakawa, Quantum mpemba effect in a quantum dot with reservoirs, *Phys. Rev. Lett.* **131**, 080402 (2023).
- [13] A. K. Chatterjee, S. Takada, and H. Hayakawa, Multiple quantum mpemba effect: exceptional points and oscillations, arXiv preprint arXiv:2311.01347 (2023).

- [14] F. Ares, S. Murciano, and P. Calabrese, Entanglement asymmetry as a probe of symmetry breaking, *Nature Communications* **14**, 2036 (2023).
- [15] R. Bao and Z. Hou, Accelerating relaxation in markovian open quantum systems through quantum reset processes, arXiv preprint arXiv:2212.11170 (2022).
- [16] S. Esposito, R. De Risi, and L. Somma, Mpemba effect and phase transitions in the adiabatic cooling of water before freezing, *Physica A: Statistical Mechanics and its Applications* **387**, 757 (2008).
- [17] M. Vynnycky and S. Mitchell, Evaporative cooling and the mpemba effect, *Heat and mass transfer* **46**, 881 (2010).
- [18] X. Zhang, Y. Huang, Z. Ma, Y. Zhou, J. Zhou, W. Zheng, Q. Jiang, and C. Q. Sun, Hydrogen-bond memory and water-skin supersolidity resolving the mpemba paradox, *Physical Chemistry Chemical Physics* **16**, 22995 (2014).
- [19] J. Jin and W. A. Goddard III, Mechanisms underlying the mpemba effect in water from molecular dynamics simulations, *The Journal of Physical Chemistry C* **119**, 2622 (2015).
- [20] S. Yang, X. Wang, and S. D. Sarma, Generic hubbard model description of semiconductor quantum-dot spin qubits, *Physical Review B* **83**, 161301 (2011).
- [21] Here, the difference between the two initial states Δa_3 and Δa_4 is set to be constant. This procedure is possible for the density matrix elements ρ_1 and ρ_2 since their values are solely determined by the initial conditions.
- [22] Supplemental material.
- [23] E. Chitambar and G. Gour, Quantum resource theories, *Reviews of modern physics* **91**, 025001 (2019).
- [24] R. Vosk and E. Altman, Dynamical quantum phase transitions in random spin chains, *Physical review letters* **112**, 217204 (2014).
- [25] S. De Nicola, A. A. Michailidis, and M. Serbyn, Entanglement view of dynamical quantum phase transitions, *Physical Review Letters* **126**, 040602 (2021).
- [26] B. Skinner, J. Ruhman, and A. Nahum, Measurement-induced phase transitions in the dynamics of entanglement, *Physical Review X* **9**, 031009 (2019).
- [27] R. Li, X. Wang, K. Zhang, and J. Wang, Page time as a transition of information channels: High-fidelity information retrieval for radiating black holes, arXiv preprint arXiv:2309.01917 (2023).
- [28] C. Batista and G. Ortiz, Generalized jordan-wigner transformations, *Physical review letters* **86**, 1082 (2001).
- [29] S. A. Hill and W. K. Wootters, Entanglement of a pair of quantum bits, *Physical review letters* **78**, 5022 (1997).
- [30] R. Horodecki, P. Horodecki, M. Horodecki, and K. Horodecki, Quantum entanglement, *Reviews of modern physics* **81**, 865 (2009).
- [31] B. Schumacher and M. D. Westmoreland, Quantum mutual information and the one-time pad, *Physical Review A* **74**, 042305 (2006).
- [32] K. Modi, A. Brodutch, H. Cable, T. Paterek, and V. Vedral, The classical-quantum boundary for correlations: Discord and related measures, *Reviews of Modern Physics* **84**, 1655 (2012).
- [33] T. Yu and J. Eberly, Sudden death of entanglement, *Science* **323**, 598 (2009).
- [34] A. Streltsov, G. Adesso, and M. B. Plenio, Colloquium: Quantum coherence as a resource, *Reviews of Modern Physics* **89**, 041003 (2017).
- [35] X. Wang and J. Wang, Nonequilibrium effects on quantum correlations: Discord, mutual information, and entanglement of a two-fermionic system in bosonic and fermionic environments, *Phys. Rev. A* **100**, 052331 (2019).
- [36] X. Wang and J. Wang, The effect of nonequilibrium entropy production on the quantum fisher information and correlations, *Quantum Information Processing* **21**, 1 (2022).
- [37] Z. Zhang, X. Wang, and J. Wang, Quantum fluctuation-dissipation theorem far from equilibrium, *Physical Review B* **104**, 085439 (2021).
- [38] P. Eastham, A. Spracklen, and J. Keeling, Lindblad theory of dynamical decoherence of quantum-dot excitons, *Physical Review B* **87**, 195306 (2013).
- [39] U. Harbola, M. Esposito, and S. Mukamel, Quantum master equation for electron transport through quantum dots and single molecules, *Physical Review B* **74**, 235309 (2006).
- [40] R. Yoshii and H. Hayakawa, Analytical expression of geometrical pumping for a quantum dot based on quantum master equation, arXiv preprint arXiv:1312.3772 (2013).